Catalysis Today 152 (2010) 17–23

Contents lists available at ScienceDirect

Catalysis Today

journal homepage: www.elsevier.com/locate/cattod

Sulfated alumina and zirconia in isobutane/butene alkylation and *n*-pentane isomerization: Catalysis, acidity, and surface sulfate species

Marina Yu. Smirnova *, Alexander V. Toktarev, Artem B. Ayupov, Gennady V. Echevsky

Boreskov Institute of Catalysis, Prosp. Akad. Lavrentieva 5, Novosibirsk 630090, Russian Federation

ARTICLE INFO

Article history:
Available online 25 September 2009

Keywords:
Sulfated alumina
Sulfated zirconia
Isobutane alkylation
Pentane isomerization
Acidity
IR spectroscopy
TPD ammonia

ABSTRACT

The catalytic behavior of sulfated alumina (SA) and zirconia (SZ) was compared for two acid-catalyzed reactions, i.e., isobutane/butene alkylation and isomerization of *n*-pentane. For the alkylation reaction, the SZ catalyst gave a higher C_{5+} alkane yield and much lower selectivity for trimethylpentanes (TMPs) at 2 h TOS. However, TMPs selectivity was comparable for both catalysts at 5.5 h TOS. For the isomerization, high *n*-pentane conversion was obtained on SZ at the reaction temperature of 100 °C when SA had no activity. Surface sulfate species were identified by IR spectroscopy. The acidity of sulfated oxides was compared by IR spectroscopy using pyridine and carbon monoxide as probe molecules and TPD–MS of ammonia. An effort was made to explain the difference between catalytic behavior of two sulfated oxides in terms of acidity, the nature of surface sulfate species and the formation of hydride species.

1. Introduction

Despite extensive studies of both physicochemical and catalytic properties of sulfated oxides, the nature of their activity in alkane transformation is still a matter of discussion. Carbenium-type intermediates are considered as an active species in most reports; however, there is controversy regarding the routes of their formation as well as the nature of sites activating paraffins on sulfated oxides. The presumed superacidity of sulfated oxides has been subject to criticism because most physicochemical methods for acidity characterization have not confirmed this hypothesis [1–3]. Therefore, reaction pathways via carbonium ion formation or H^- abstraction by acidic sites of sulfated oxides seem unlikely. As an alternative to these pathways, non-acidic activation through the oxidation of alkane, including one-electron oxidation, has been proposed [4,5]. In this case, sulfate or pyrosulfate species are considered to be oxidizing agents [4,5]. However, alkane oxidation is accompanied by the reduction of sulfate species to SO_2. In the case of the catalytic route of alkane activation, re-oxidation of the reduced sulfur species is needed: otherwise, such a pathway should be considered as a non-catalytic one. Efforts have been made to explain the relatively long "lifetime" of SZ in the case of non-catalytic activation [6,7]. However, the acidic mechanisms should still be considered as a possible route of alkane activation.

Because extremely high activity of sulfated oxides in alkane transformations cannot be derived from the strength of their Broensted or Lewis acid sites, surface stabilization of the transition state complex [2], increase of Broensted site strength by adjacent Lewis sites [8,9] and concerted mechanism via multiple sites [10,11] have been proposed in the framework of acidic alkane activation. Additionally, high surface density of acid sites on the sulfated oxides, especially compared with zeolites, proposed to be responsible for their high catalytic activity [12].

Thus, different authors consider different possibilities of alkane activation on sulfated oxides. These possibilities can be provided by the means of surface sulfate species, Broensted/Lewis paired sites or Lewis sites and suitably positioned surface sulfate groups, which enable the concerted mechanism. In this paper, we consider different routes of alkane activation on sulfated oxides and attempt to identify the most probable route based on a comparative study of acidic properties, structure of sulfate species and catalytic behavior of two sulfated oxides (alumina and zirconia) in two acid-catalyzed reactions (isoparaffin/olefin alkylation and alkane isomerization).

The choice of sulfated oxides is based on the large difference between the activities of these catalysts in the aforementioned reactions reported in literature [13,14]. Much higher activity in both alkylation and isomerization has been obtained for SZ in comparison with SA. The lower activity of SA has been explained by its lower acid site strength, as determined by the method of Hammett indicators [13] and some other methods for the acid sites strength characterization [14,15]. However, it should be noted that the surface area of SA is often much greater than that of other

* Corresponding author. Tel.: +7 383 3269589; fax: +7 383 3309827.
E-mail addresses: smirnova@catalysis.ru (M.Yu. Smirnova), atok@catalysis.ru (A.V. Toktarev), artem@catalysis.ru (A.B. Ayupov), egv@catalysis.ru (G.V. Echevsky).

0920-5861/$ – see front matter © 2009 Elsevier B.V. All rights reserved.
doi:10.1016/j.cattod.2009.08.013

sulfated oxides. Because of this, a similar sulfation procedure (i.e., concentration of sulfate precursor) used for precursors of zirconia and alumina should produce a surface sulfate concentration on SA that is too low in comparison with that on SZ. Because the activity of sulfated oxides strongly depends on the sulfate content [16,17], the catalytic behavior, as well as the acidic properties, should be compared for samples with close surface sulfate content. This comparative investigation was done in the present paper.

As mentioned above, the isobutane/butene alkylation and *n*-pentane isomerization were used to test catalytic properties of SA and SZ. Despite the fact that both reactions can be considered as acid-catalyzed, the role of acid sites in these reactions is proposed to be different. The alkylation reaction is catalyzed by strong Broensted sites of solid acids [18]. In the case of alkane isomerization proceeding via a bimolecular mechanism, Broensted sites are reported to be essential at the stage of olefin protonation [4,19]. However, the role of acid sites in alkane activation (i.e., olefin formation) is a matter of debate.

2. Experimental

2.1. Catalyst preparation and characterization

The SA sample was prepared by treatment of γ-alumina (surface area 229 $m^2\,g^{-1}$, pore volume 0.39 $cm^3\,g^{-1}$) with an aqueous solution of H_2SO_4 as described elsewhere [16]. The SZ catalyst was prepared from an ammonia complex of zirconium hydroxycarbonate according to Ref. [20]. The composition and preparation conditions of sulfated samples are presented in detail in Table 1. Sulfate content was measured as sulfur on a Vario EL III CHNOS Elemental analyzer. BET surface areas were determined with N_2 at −196 °C on a static volumetric instrument Autosorb-1-C (Quantachrome Instruments).

2.2. Infrared spectroscopy

FTIR measurements were performed on a Varian Scimitar 1000 FTIR spectrometer equipped with a high-temperature flow cell with NaCl windows. A self-supported wafer with a density of 10 mg cm^{-2} in the case of the SA sample (20 mg cm^{-2} in the case of SZ) was gradually heated at a rate of 5 °C min^{-1} to 450 °C. It was then cooled to 150 °C, and IR spectra were recorded. Pyridine adsorption tests in IR study of surface sulfate groups were carried out at 150 °C by injecting of 10 μL of pyridine into the gas line through a septum injection port. After pyridine adsorption, the sample was purged at the same temperature with high-purity helium for 1 h, and a spectrum was collected.

To estimate the concentration of Broensted and Lewis acid sites, IR spectra of adsorbed pyridine in vacuum were obtained. Samples, in the form of self-supported wafers, were pretreated in vacuum for 2 h at 400 °C and exposed to pyridine (10 Torr) at 150 °C for 30 min. The excess of pyridine was removed by evacuation at the same temperature for 30 min.

IR spectra of adsorbed CO were recorded on a Shimadzu FTIR-8300 spectrometer at the temperature of liquid nitrogen with a resolution of 4 cm^{-1}. For IR studies, wafers were pretreated as described above. Different CO pressures (0.2–10 Torr) were introduced stepwise at the temperature of liquid nitrogen up to the pressure of 10 Torr. All spectra presented in paper were normalized to the thickness of wafers.

The temperature-programmed desorption of ammonia (TPD) experiments were carried out on a static volumetric instrument Autosorb-1-C equipped with a mass spectrometer (QMS 200 Prisma). For these experiments 0.5 g of catalysts were pretreated in oxygen flow at 550 °C for 1 h, followed by cooling down to 100 °C. The system was then purged with helium, and ammonia was adsorbed at 100 °C for 10 min. Physically adsorbed NH_3 was removed by evacuation at the same temperature for 2 h. From the temperature of evacuation, the system was heated to 570 °C at a rate of 10 °C min^{-1} and was held at the final temperature for 1 h, while a helium flow (36 ml min^{-1}) was passing through the reactor. TPD–MS profiles were generated by plotting the intensities of the signals at m/z 16 (responsible for NH_3) and m/z 64 (SO_2) versus time or temperature.

2.3. Catalytic test

The alkylation experiments were carried out in an autoclave with agitation at the temperature of 50 °C and total pressure of 0.9 MPa. Each sample was activated "ex-situ" at 550 °C for 1 h in air before starting the reaction runs. After activation, hot catalyst (2 g) was loaded into an autoclave filled with argon; the autoclave was then sealed and charged with isobutane (13 g). After that, isobutane/*n*-butene feed with an i/o molar ratio of 4.5 being maintained in the liquid phase under argon pressure was fed into the autoclave ($WHSV_{C4=}$ of 0.24 h^{-1}). The catalytic parameters were calculated using product compositions from the gas chromatographic analysis. The alkylate yield was defined as total concentration of C_{5+} products divided by the amount of butene reacted. The TMP selectivity was calculated by dividing the total TMP concentration by the total concentration of C_{5+} products.

Isomerization of *n*-pentane was carried out in a fixed bed reactor at atmospheric pressure and two different temperatures (100 and 200 °C). Precalcined sample (3 g) was loaded into the reactor (10 mm i.d.) and activated in situ at 450 °C for 1 h in helium flow. After the activation, the sample was cooled to the reaction temperature, and the reaction mixture (0.01% or 0.57% *n*-pentane in helium, total flow of 7 ml/min) was flown through the catalyst bed. The concentration of olefinic impurities in *n*-pentane was less than 10 ppm. Analysis of the reaction products was performed by on-line chromatography using flame ionization detection. The activity was shown through *n*-pentane conversion.

3. Results

3.1. Catalytic properties of SA and SZ

The catalytic properties of SZ and SA samples for isobutane/butene alkylation are summarized in Table 2. It can be seen that the alkylate yield per olefin observed for SZ at 2 h TOS is higher than that for SA and exceeds the theoretical yield corresponding to the stoichiometry of alkylation (204 wt.%). The alkylate yield above the

Table 1
Composition and preparation conditions of sulfated samples.

Sample	$T_{calcination}$ (°C)	S_{BET} ($m^2\,g^{-1}$)	C(SO_4)	
			(wt%)	(μmol m^{-2})
SA	550	175	16.9	10.1
SZ	620	164	14.1	8.9

Table 2
Catalytic properties of SA and SZ in isobutane/butene alkylation.

Sample	SA		SZ	
TOS (h)	2	5.5	2	5.5
C_4= conversion (wt%)	99.9	96.8	99.8	97.9
Alkylate yield (wt%)	203	197	280	227
C_3 selectivity (wt%)	<1	1.3	<1	<1
C_5–C_7 selectivity (wt%)	34	20	89	39
C_8 selectivity (wt%)	50	62	9	43
TMPs selectivity (wt%)	32	48	5	33
i-C_5/(C_6+C_7) (mol mol^{-1})	1.6	1.1	3.4	1.9

theoretical one can be evidence both for high cracking of alkylation products [21] and isobutane self-alkylation [22]. It can be concluded that such reactions are not typical for SA because the alkylate yields obtained for this sample do not exceed the theoretical one. The higher C_5–C_7 product selectivity and much lower selectivity for TMPs at 2 h TOS are observed on SZ in comparison with SA. The evolution of these products with TOS is similar for both sulfated oxides. It is characterized by a decrease in C_5–C_7 products and an increase in TMPs selectivity, which becomes comparable for both samples. Isopentane being the predominant compound among C_5–C_7 products is noteworthy, and its selectivity at 2 h TOS considerably exceeds that for TMPs in the case of SZ. In addition, the molar ratio of i-C_5/(C_6 + C_7) obtained on SZ after 2 h TOS is too high to be explained by C_8 products cracking in accordance with Ref. [21]. It can be concluded in this case that the majority of isopentane is the result of the cracking of C_{9+} products [23,24] formed by multiple addition of an olefin to the carbocation due to slow hydride abstraction [23,25].

The *n*-pentane conversion obtained on two sulfated oxides via isomerization is reported in Fig. 1. As can be seen, SZ demonstrates a very high conversion at the temperature of 100 °C when SA has no activity. SA sample exhibits an appreciable *n*-pentane conversion (6%) only at 200 °C. However, practically total conversion of *n*-pentane is observed for SZ at this temperature. To obtain comparable conversions on these sulfated oxides, a much higher *n*-pentane concentration in helium mixture had to be used for SZ in comparison with SA sample.

3.2. IR spectroscopy of adsorbed pyridine

Fig. 2 presents segments of IR spectra (in the 1400–1700 cm^{-1} range) of pyridine (py) adsorbed on SA and SZ samples. Strong IR adsorption bands observed in the spectrum of SZ at 1611 (ν_{8a}) and 1445 (ν_{19b}) cm^{-1} (at 1623 and 1454 cm^{-1} in the case of SA) are characteristic of py coordinated to Lewis acidic centers. It should be noted that the position of these bands is slightly different for various sulfated oxides. However, this fact provides no evidence for differences in the Lewis site strength because the application of the ν_{8a} band position as a measure of Lewis site strength is permitted only for catalysts of similar chemical nature [26]. Broad adsorption bands around 1640 (ν_{8a}) and 1544 (ν_{19b}) cm^{-1} correspond to py interacting with Broensted acid sites. To obtain quantitative information from the spectral data of py adsorption, the molar absorption coefficients for the analytical 19b mode of py species were used [27]. These data are reported in Table 3. One can see in

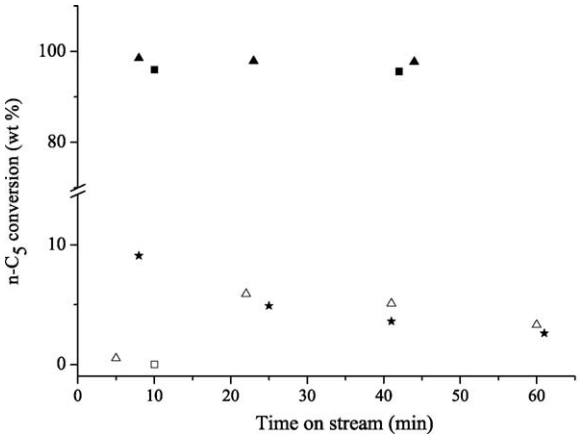

Fig. 1. Isomerization of *n*-pentane (7 ml/min 0.01% *n*-pentane in He) over SA (open symbols) and SZ (filled symbols) catalysts at different reaction temperatures: 100 °C (squares), 200 °C (triangles). Isomerization of *n*-pentane (7 ml/min 0.57% *n*-pentane in He) over SZ at 200 °C (stars).

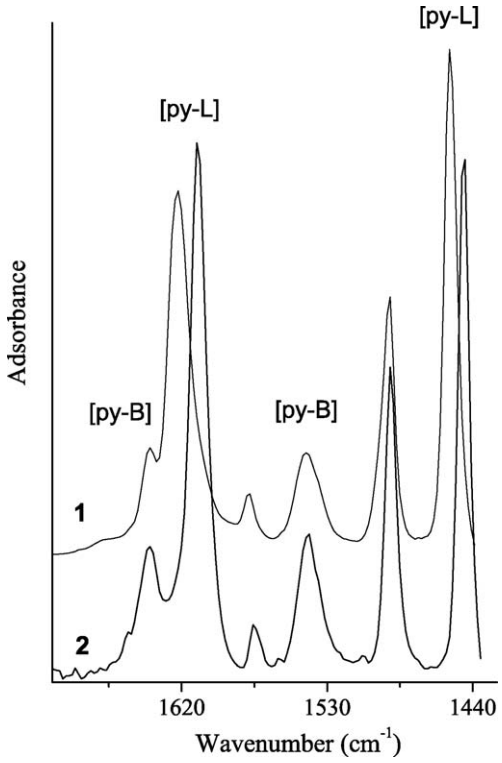

Fig. 2. IR spectra of pyridine adsorbed at 150 °C on SA and SZ samples: (1) SA sample; (2) SZ sample.

Table 3
Amount of Lewis and Broensted sites (mmol g^{-1}) calculated from the IR spectra of adsorbed py.

Sample	L	B	L/B
SA	0.126	0.057	2.2
SZ	0.125	0.066	1.9

Table 3 that the amount of Lewis sites is similar for both catalysts. The amount of Broensted sites on SZ slightly exceeds that on SA.

3.3. IR spectroscopy of adsorbed CO

The weak basicity makes CO a suitable probe to discriminate between acid sites of different strengths. The interaction of CO molecule with the surface of the catalyst results in an upward shift of the C–O stretching frequency ($\Delta\nu_{CO}$) from the value corresponding to gaseous CO. The value $\Delta\nu_{CO}$ can be used as a measure of strength of aprotic acid sites in accordance with Ref. [28]. When CO is adsorbed at liquid nitrogen temperature, several types of adsorbed species can be observed: bands in the spectral range of 2240–2190 cm^{-1} corresponding to CO adsorbed on strong cationic sites, bands in the spectral range of 2200–2170 cm^{-1} due to CO adsorbed on weaker Lewis sites and bands in the spectral range of 2175–2145 cm^{-1} corresponding to CO interacting with acidic OH groups [29].

IR spectra of CO adsorbed at liquid nitrogen temperature on the sulfated samples are reported in Fig. 3. The band at 2204–2207 cm^{-1} is assigned to the strongest Lewis sites on SZ (Fig. 3A). For the SZ sample, the band frequencies corresponding to Lewis sites and relative intensities of CO bands assigned to Broensted and Lewis sites are close to data reported by other authors for SZ spectra recorded under similar conditions [30,31]. The strongest Lewis sites on SA are characterized by the band at 2210–2214 cm^{-1}

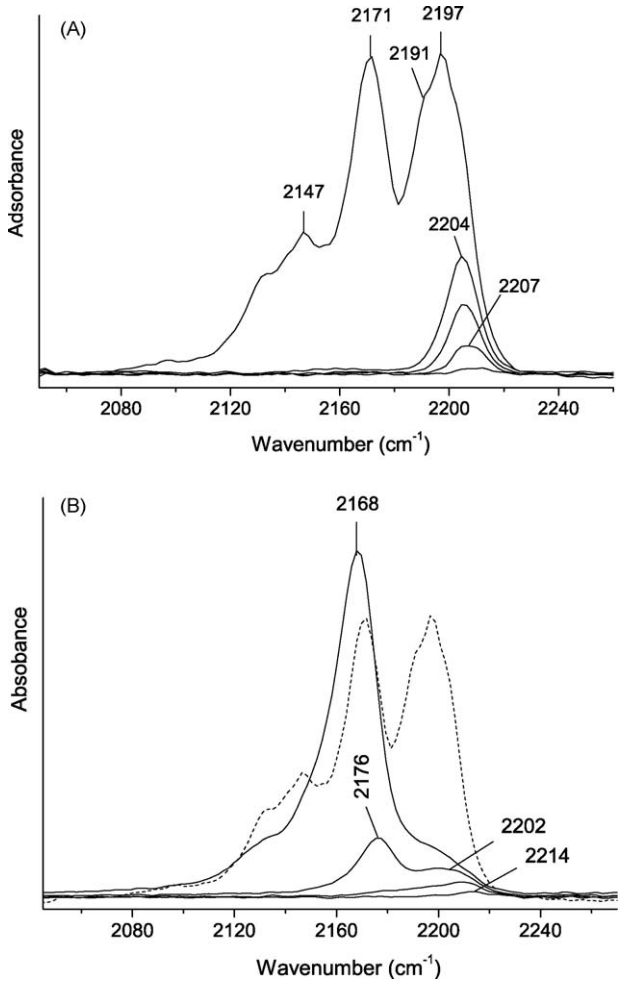

Fig. 3. Low-temperature IR spectra of CO adsorbed on SZ (A) and SA (B) samples at CO pressure from 0.2 to 10 Torr. The dotted line corresponds to the IR spectra of SZ after adsorption of 10 Torr CO.

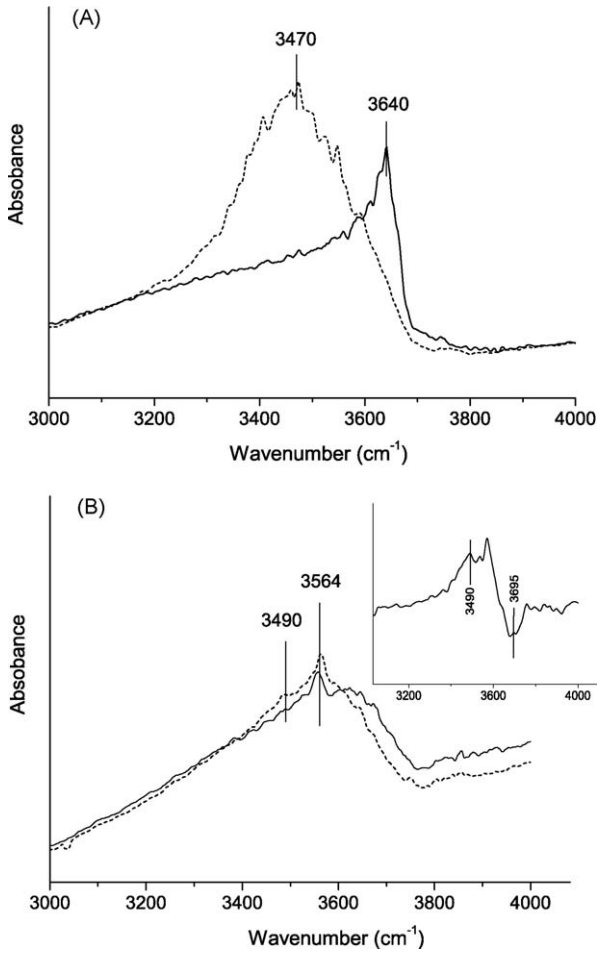

Fig. 4. O–H stretching region of SZ (A) and SA (B) samples before (solid line) and after (dashed line) CO adsorption at liquid nitrogen temperature. Insert shows differential spectra.

(Fig. 3B), the frequency of which exceeds that corresponding to the strongest Lewis sites on SZ. However, a significant difference between intensities of CO band centered around 2200 cm^{-1} is observed for various sulfated oxides (Fig. 3B). Based on similar values of molar absorption coefficients for the CO band around 2200 cm^{-1} reported for zirconia and alumina [32], it can be concluded that a much higher amount of Lewis sites exists on SZ in comparison with SA. However, this fact is inconsistent with data obtained from the IR spectra of adsorbed pyridine. Although pyridine as a probe molecule for testing acidity is well accepted, its application for evaluation of Lewis acidity of oxidic systems containing surface anions has been subject to criticism because of strong interaction between adsorbed pyridine and surface sulfate species [33]. Therefore, it is probably more correct to compare Lewis sites amount on different sulfated oxides using IR spectroscopy of adsorbed CO.

Interaction of CO at liquid nitrogen temperature with surface hydroxyls is found to shift the O–H stretching frequency due to the formation of hydrogen-bonded complexes. The value of the downward shift ($\Delta\nu_{OH}$) is used as a measure of Broensted site strength. Fig. 4 shows that adsorption of CO results in a larger shift of O–H band of SA ($\Delta\nu_{OH}$ = 205 cm^{-1}), which is indicative of higher Broensted site strength on this sample in comparison with SZ ($\Delta\nu_{OH}$ = 170 cm^{-1}). It should be noted that the value of the downward shift obtained for SZ sample is in a good agreement with the values, $\Delta\nu_{OH}$ from 140 to 220 cm^{-1}, reported by other authors [30,31,34]. However, in accordance with the data reported in Ref. [2], the Broensted acid sites of sulfated samples are weaker than are those of zeolites.

3.4. Temperature-programmed desorption of ammonia

Although TPD of adsorbed bases is commonly used to measure acid site distribution of solid acids like zeolites, many authors argue that this method is not a suitable technique for evaluation of acidic properties of sulfated oxides because of emission of volatile products that are not originated from the base desorption [1,35,36]. To discriminate between desorbing base and evolved SO_2 due to sulfate group decomposition, a mass-spectrometer was used to track the evolved species during TPD experiment. TPD–MS profiles for SZ and SA samples shown in Fig. 5 demonstrate that ammonia desorption from both samples results in a broad peak with a maximum near 300 °C. The majority of ammonia desorbs from both sulfated oxides at a temperature below than 550 °C, whereas SO_2 evolution begins near 500 °C. To avoid thermal decomposition of sulfate, the final temperature of TPD experiments is only slightly greater than the calcination temperature of the SA sample. Therefore, to observe the peak corresponding to SO_2 evolution, TPD–MS time profiles are presented in Fig. 5 (inserts). The elemental analysis of the sulfated samples after TPD experiments exhibits reduced sulfate contents of SZ and SA samples, with the decrements of 8.8 and 1.5%, respectively. These data are consistent with the intensities of the TPD–MS peak corresponding to SO_2 evolution. It is noteworthy that this peak is

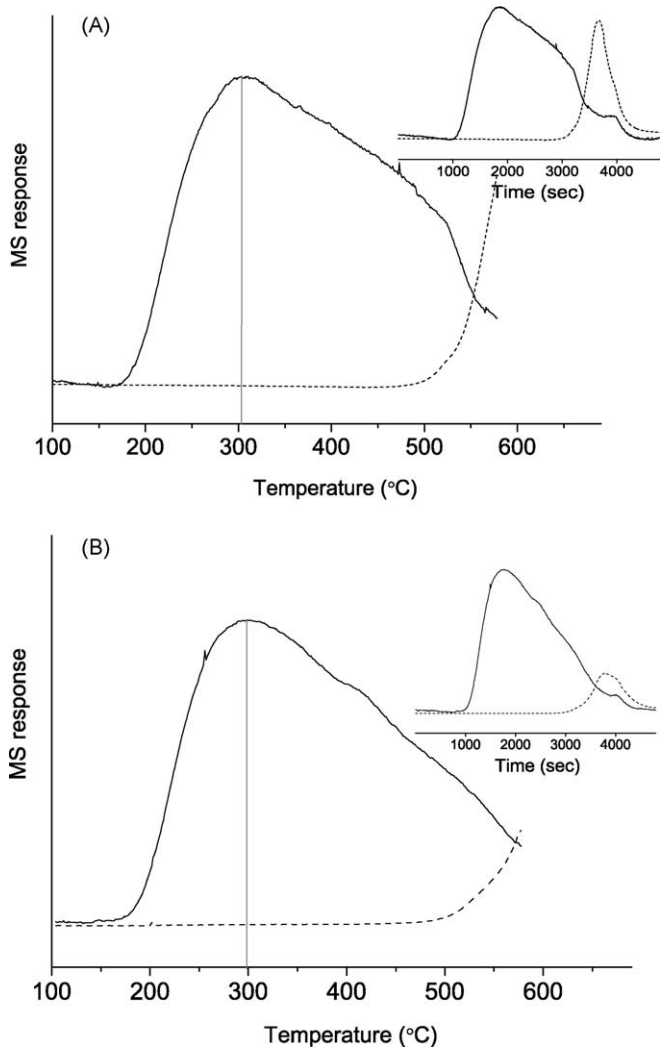

Fig. 5. TPD–MS temperature profiles obtained for SZ sample (a) and SA sample (b). Solid curves denote NH_3 evolution and dashed curves denote SO_2 evolution. Inserts show TPD–MS time profiles.

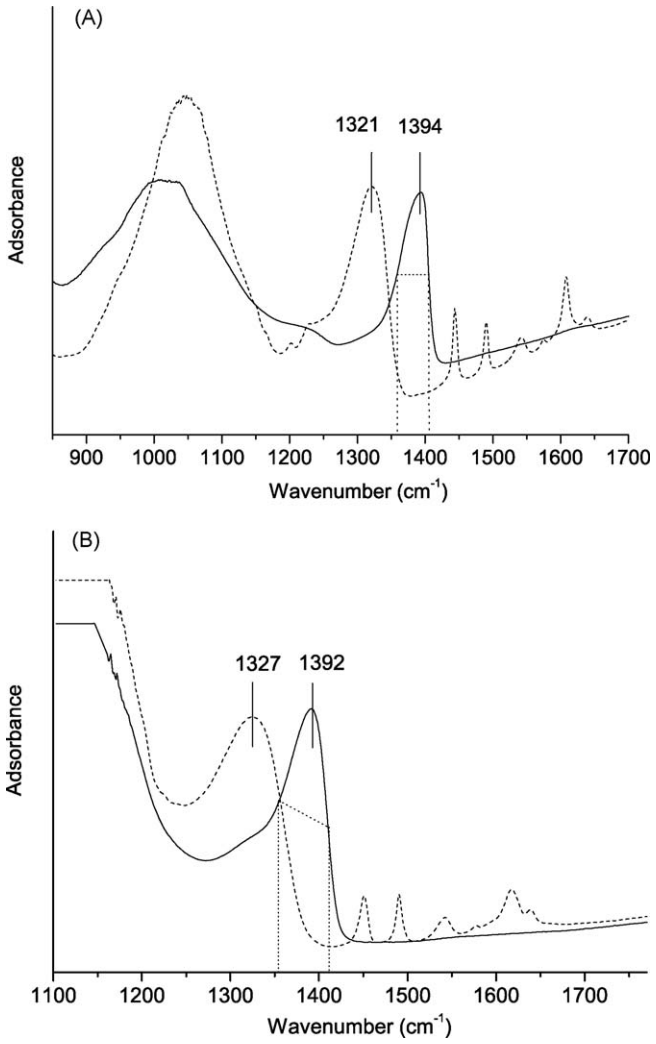

Fig. 6. IR spectra in the sulfate-stretching region for SZ (A) and SA (B) samples. Dashed-line traces show the spectral profiles after py adsorption at 150 °C.

not observed for the SZ sample during the TPD blank experiment (without pre-adsorbed ammonia). In accordance with literature data, SO_2 evolution is associated with a redox reaction between the sulfate group and the adsorbate molecule [1]. However, before the redox reaction, the formation of an intermediate complex between the adsorbate molecule and the surface sulfate group via a Lewis site is assumed [36]. Some portion of the base molecules desorbs from these sites during heating. Another portion is proposed to be converted to surface species consisting of a base molecule bonded with a sulfate group. Further heating leads to formation of oxidation products from these surface species [36]. In line with this data, more intensive SO_2 formation can be caused by a higher amount of Lewis sites and by stronger interaction between ammonia and sulfate species via Lewis sites of SZ in comparison with those of SA. Moreover, the one-electron oxidizing ability of SZ should be considered as a possible reason [37].

3.5. IR spectra in the region of SO stretching frequencies

Fig. 6 presents IR spectra of surface sulfate groups of the SZ and SA samples activated at 450 °C. Spectra of the SZ sample exhibit two groups of bands in the 1300–1440 and 900–1170 cm^{-1} regions, which are attributed to S=O stretching frequencies ($\nu_{S=O}$) and stretching modes of S–O bonds, respectively [38,39]. Only the S=O stretching region is seen in the spectra of the SA sample because of the strong absorbance of alumina at the frequencies below than 1200 cm^{-1}. The peak at 1390–1400 cm^{-1} demonstrates that both sulfated samples are composed of highly covalent sulfate species with the S=O bond order close to 1.9 [14]. The multiplicity of this peak is explained by the surface heterogeneity and the occurrence of both isolated sulfate species with $\nu_{S=O} < 1400\ cm^{-1}$ and of pyrosulfate species with $\nu_{S=O} \geq 1400\ cm^{-1}$ [34,40–42]. It can be seen in Fig. 6 that the 1400 cm^{-1} component is included in the peak of highly covalent sulfate species in the spectra of both sulfated samples. However, we are not able to make an accurate comparison of intensities of this band for different sulfated oxides because of the strong absorbance of alumina and unknown individual molar absorption coefficients.

The drastic shift of IR bands in the SO stretching region observed after py adsorption is evidence for a strong interaction between adsorbed py molecules and surface sulfates. It demonstrates the ability of surface sulfate groups to absorb electrons from a basic molecules with subsequent reduction of the S=O bond order. It is proposed that this interaction is realized via a metal cation bonded with surface sulfate group [14]. The shifts reported for SZ and SA by Jin et al. are about 51 and 33, respectively [14]. The values of shifts that are well-correlated with activity of these sulfated oxides in isomerization of cyclopropane have been demonstrated by these

authors. Despite a substantial difference between activities of our sulfated samples in *n*-pentane isomerization, no significant difference is seen in the values of the shifts (Fig. 6). The comparable sulfate contents obtained for SZ and SA samples in the present work in contrast with those in [14] can be the reason for more comparable values of the shifts.

4. Discussion

In Section 1, we discuss three probable mechanisms by which activation of paraffins may occur. Those are the activation by a highly acidic Broensted site followed by a carbonium ion formation, the elimination of a hydride ion by a strong Lewis site with a subsequent carbenium ion formation, and the oxidation by sulfate groups.

The comparison of catalytic activity of SA and SZ for *n*-pentane isomerization reaction shows that SZ is a superior catalyst. Its activity at 100 °C is much greater than that of SA at 200 °C. To explain this fact, we have made studies of surface sulfate species and acidic properties of these catalysts. The amounts of both Broensted and Lewis sites measured by IR of adsorbed pyridine are found to be comparable for these sulfated oxides. IR study of CO adsorption demonstrates that the strength of acid sites (both Broensted and Lewis) on SA is not lower and even slightly higher than that on SZ. Therefore, the difference in isomerization activities of SA and SZ samples cannot be explained by differences in strength or amount of Broensted acid sites. However, based on the results of IR of adsorbed CO, it is proposed that there is a higher amount of Lewis sites on SZ in comparison with SA. In accordance with one of the hypotheses, the strength of Broensted sites can be increased by the electron-withdrawing ability of adjacent Lewis sites [8,9,19]. One may speculate in this case that larger amount of Lewis sites on SZ produces a larger amount of highly acidic Broensted sites in comparison with SA. The assumption of Lewis site influence on Broensted site strength derives from the experimental data, which demonstrate that the simultaneous presence of acid sites of both types is vital for the catalytic activity of SZ [3,8,9]. However, no other experimental evidence of such paired sites has been obtained. Moreover, the selective poisoning experiments with adsorbed ammonia on the surface of SZ show only a diminution of catalytic activity but not a complete deactivation [11]. The facts discussed above lead to conclusion that alkane activation by Broensted sites is an unlikely route in the case of sulfated oxides.

Oxidative activation of paraffins seems more feasible than the aforementioned route, as large amounts of evidence for this have been reported: emission of SO_2 during TPD of bases [1] and TPDR of *n*-C_4 [7,43], and formation of oxygenated compounds after hydrocarbon transformations on sulfated oxides [5,44,45]. It has been argued that highly covalent surface sulfate or pyrosulfate species characterized by an S=O vibration at 1390–1410 cm^{-1} play a key role in alkane activation [41,46]. However, a comparison of IR spectra of our sulfated samples in the region of SO stretching frequencies shows similar band of highly covalent sulfate species at 1390–1400 cm^{-1}. Therefore, the alkane oxidation by surface sulfate groups seems unlikely to be the main route of alkane activation on highly active sulfated oxides. It is also noteworthy that the formation of oxygenated compounds from alkanes on sulfated oxides is predominantly observed at the temperatures not less than 200 °C [7,45]. Moreover, the reduction of the oxidation state of sulfur should lead not only to a deactivation of oxidative sites but also to a decrease in concentration of strong acid sites [47,48].

Let us now consider a possibility of a third mechanism, in which Lewis sites participate in alkane activation. As mentioned above, sulfated oxides of alumina and zirconia have similar surface sulfate species and comparable Broensted acidities. In contrast, the amount of Lewis acid sites on SZ obtained by IR of adsorbed CO is higher in comparison with that on SA. In terms of the mechanism under consideration, this fact is in agreement with the higher isomerization activity observed for the SZ sample. Because the Lewis sites on sulfated oxides are not particularly strong and their strength does not exceed that on γ-Al_2O_3 [2,3], alkane activation by Lewis sites may be realized only via a concerted mechanism [10]. In accordance with this mechanism, the hydride ion abstraction, followed by the formation of surface hydride, occurs on Lewis sites with the assistance of adjacent sulfate groups, which contribute to the stabilization of the transition state and transfer a proton to yield the olefin. It is noteworthy that the formation of Zr–H species after *n*-alkane adsorption has been detected by IR spectroscopy [49]. Moreover, the shift of IR bands in the SO stretching frequencies that is observed after adsorption of strong bases (pyridine, ammonia) is evidence for the interaction between the adsorbed molecule and the surface sulfate. It is assumed that this interaction is realized via a metal cation bonded with a surface sulfate group [14,36]. Because such shift is observed after adsorption of paraffins on sulfated zirconia and iron oxide [43,49], it can be concluded that adsorption of paraffins occurs on Lewis sites coupled with a surface sulfate group.

In addition to the activation mechanism where cationic sites participate in hydride abstraction, an oxidative mechanism of alkane activation by cationic sites has been proposed for SZ [37]. According to this mechanism, Zr^{4+} surface species act as a one-electron oxidant for the alkane molecule. Sulfate groups are proposed as hydrogen acceptors in this mechanism in contrast to the oxidative mechanism mentioned above, where they play a key role. It should be noted that both activation mechanisms in which cationic sites take part are not easily distinguishable from each other because the same experimental data (for example, Zr^{3+} formation after *n*-C_4 adsorption on SZ) can be indicative of both mechanisms [37,50].

In summary, it may be said that the combination of the Lewis site and the surface sulfate group is the most probable active site for catalytic alkane activation. In line with this assumption, two reasons can be proposed to explain the much lower SA activity in paraffin isomerization in comparison with SZ: a lower feasibility of alkane activation by Lewis sites of SA or a predominant role of the oxidative (non-catalytic) mechanism of paraffin activation for SA catalysts.

In addition to the difference in catalytic activity between SA and SZ samples for *n*-pentane isomerization, the difference in the initial catalytic behavior of these catalysts in the alkylation reaction has been also noted. The alkylate yield obtained for SZ at 2 h TOS does not correspond to the stoichiometry of isobutane/butene alkylation reaction and can be considered to be a result of isobutane self-alkylation. In contrast to SZ, self-alkylation is not typical for SA. It seems reasonable that during the initial time of the reaction, when the surface of sulfated samples is covered by preliminary adsorbed isobutane, the state of catalyst surface is similar to that during the induction period of isomerization. The addition of olefin, with subsequent formation of a carbenium cation on Broensted sites, induces the transformation of isobutane itself. This assumption is in line with literature data regarding isomerization. The buildup of olefins and their accumulation on the surface is considered to be the reason for the induction period observed during isomerization in accordance with Refs. [51,52]. Moreover, it is found that an increase of activity of SZ in *n*-butane isomerization can be caused by the addition of different C_2–C_5 olefins [52]. In the case of SA, the contribution of isobutane self-alkylation is negligible, which is in good agreement with the low activity of this sulfated oxide in isomerization. It is probable that self-alkylation is the prevailing route at initial reaction times in the case of SZ. With increasing TOS, the contribution of self-alkylation decreases drastically. Therefore,

the catalytic parameters for the SZ sample at 5.5 h TOS are comparable with the catalytic parameters observed for SA. As already noted, the self-alkylation over SZ is accompanied by extremely high selectivity towards isopentane. It is concluded that such high selectivity could not be explained by C_8 products cracking and can be originated from cracking of C_{9+} products [23,24]. The formation of these products is considered to be a result of multiple addition of an olefin to the carbocation due to slow hydride transfer [23,25]. Therefore, we suggest that intensive self-alkylation leads to appropriate conditions for aforementioned reactions, followed by formation of C_{9+} products. These hydrocarbons can further transform via two routes: cracking or hydride ion abstraction with subsequent formation of highly unsaturated hydrocarbon blocked acidic sites.

5. Conclusions

Based on the comparative study of acidic and catalytic properties of sulfated alumina and zirconia in isobutane/butene alkylation and *n*-pentane isomerization, it is concluded that activities of these catalytic systems are comparable in the alkylation reaction in agreement with their comparable Broensted acidities. However, a significant difference between activities of these sulfated oxides is observed for alkane isomerization. The reason of such difference is due to more feasible alkane activation by Lewis sites on SZ coupled with surface sulfate group.

Acknowledgements

The authors are indebted to Urguntsev G.A. (The Boreskov Institute of Catalysis) for preparing the SZ catalyst.

References

[1] X. Song, A. Sayari, Catal. Rev. -Sci. Eng. 38 (1996) 329.
[2] V. Adeeva, J.W. de Haan, J. Jänchen, G.D. Lei, V. Schünemann, L.J.M. van de Ven, W.M.H. Sachtler, R.A. van Santen, J. Catal. 151 (1995) 364.
[3] C. Morterra, G. Cerrato, V. Bolis, S.D. Ciero, M. Signoretto, J. Chem. Soc., Faraday Trans. 93 (1997) 1179.
[4] C. Breitkopf, H. Papp, X. Li, R. Olindo, J.A. Lercher, R. Lloyd, S. Wrabetz, F.C. Jentoft, K. Meinel, S. Förster, K.-M. Schindler, H. Neddermeyer, W. Widdra, A. Hofmann, J. Sauer, Phys. Chem. Chem. Phys. 9 (2007) 3600.
[5] A. Ghenciu, D. Fărcaşiu, J. Mol. Catal. A 109 (1996) 273.
[6] S. Hammache, J.G. Goodwin Jr., J. Catal. 211 (2002) 316.
[7] X. Li, K. Nagaoka, L.J. Simon, R. Olindo, J.A. Lercher, A. Hofmann, J. Sauer, J. Am. Chem. Soc. 127 (2005) 16159.
[8] P. Nascimento, C. Akratopoulou, M. Oszagyan, G. Coudurier, C. Travers, J.F. Joly, J.C. Vedrine, Stud. Surf. Sci. Catal. 75 (1993) 1185.
[9] A. Clearfield, G.P.D. Serrette, A.H. Khazi-Syed, Catal. Today 20 (1994) 295.
[10] M. Signoretto, F. Pinna, G. Strukul, P. Chies, G. Cerrato, S. Di Ciero, C. Morterra, J. Catal. 167 (1997) 522.
[11] Z. Hong, K.B. Fogash, J.A. Dumesic, Catal. Today 51 (1999) 269.
[12] N. Katada, J. Endo, K. Notsu, N. Yasunobu, N. Naito, M. Niwa, J. Phys. Chem. B 104 (2000) 10321.
[13] K. Satoh, H. Matsuhashi, K. Arata, Appl. Catal. A 189 (1999) 35.
[14] T. Jin, T. Yamaguchi, K. Tanabe, J. Phys. Chem. 90 (1986) 4794.
[15] D.J. Coster, A. Bendada, F.R. Chen, J.J. Fripiat, J. Catal. 140 (1993) 497.
[16] M.Yu. Smirnova, G.A. Urguntsev, A.B. Ayupov, A.A. Vedyagin, G.V. Echevsky, Appl. Catal,. A 344 (2008) 107.
[17] D. Fărcaşiu, J.Q. Li, S. Cameron, Appl. Catal., A 154 (1997) 173.
[18] A. Feller, I. Zuazo, A. Guzman, J.O. Barth, J.A. Lercher, J. Catal. 216 (2003) 313.
[19] S.X. Song, R.A. Kydd, J. Chem. Soc. Faraday Trans. 94 (1998) 1333.
[20] Patent RU 2306175 (2007).
[21] X. Xiao, J.W. Tierney, I. Wender, Appl. Catal. A 183 (1999) 209.
[22] US Patent 4 138 444 (1979).
[23] F. Cardona, N.S. Gnep, M. Guisnet, G. Szabo, P. Nascimento, Appl. Catal. A 128 (1995) 243.
[24] A. Corma, A. Martínez, C. Martínez, J. Catal. 149 (1994) 52.
[25] A. Corma, A. Martínez, Catal. Rev. -Sci. Eng. 35 (1993) 483.
[26] E.A. Paukshtis, R.I. Soltanov, E.N. Yurchenko, React. Kinet. Cat. Lett. 19 (1982) 105.
[27] C.A. Emeis, J. Catal. 141 (1993) 347.
[28] E.A. Paukshtis, R.I. Soltanov, E.N. Yurchenko, React. Kinet. Cat. Lett. 16 (1981) 93.
[29] C. Morterra, G. Cerrato, M. Signoretto, Catal. Lett. 41 (1996) 101.
[30] D. Spielbauer, G.A.H. Mekhemer, M.I. Zaki, H. Knözinger, Catal. Lett. 40 (1996) 71.
[31] O.V. Manoilova, R. Olindo, C. Otero Areán, J.A. Lercher, Catal. Commun. 8 (2007) 865.
[32] R.I. Soltanov, E.A. Paukshtis, E.N. Yurchenko, Kinet. Catal. 23 (1982) 164.
[33] C. Morterra, G. Cerrato, Phys. Chem. Chem. Phys. 1 (1999) 2825.
[34] E.E. Platero, M.P. Mentruit, C. Otero Areán, A. Zecchina, J. Catal. 162 (1996) 268.
[35] E.C. Sikabwe, M.A. Coelho, D.E. Resasco, R.L. White, Catal. Lett. 34 (1995) 23.
[36] J.S. Lee, D.S. Park, J. Catal. 120 (1989) 46.
[37] C.R. Vera, J.C. Yori, J.M. Parera, Appl. Catal. A 167 (1998) 75.
[38] C. Morterra, G. Cerrato, F. Pinna, M. Signoretto, G. Strukul, J. Catal. 149 (1994) 181.
[39] T. Yamaguchi, T. Jin, K. Tanabe, J. Phys. Chem. 90 (1986) 3148.
[40] C. Morterra, G. Cerrato, V. Bolis, Catal. Today 17 (1993) 505.
[41] X. Li, K. Nagaoka, R. Olindo, J.A. Lercher, J. Catal. 238 (2006) 39.
[42] A. Hofmann, J. Sauer, J. Phys. Chem. B 108 (2004) 14652.
[43] J.S. Lee, M.H. Yeom, D.S. Park, J. Catal. 126 (1990) 361.
[44] D. Fărcaşiu, A. Ghenciu, J.Q. Li, J. Catal. 158 (1996) 116.
[45] M. Hino, S. Kobayashi, K. Arata, React. Kinet. Cat. Lett. 18 (1981) 491.
[46] X. Li, K. Nagaoka, J.A. Lercher, J. Catal. 227 (2004) 130.
[47] J.C. Yori, J.C. Luy, J.M. Parera, Appl. Catal. 46 (1989) 103.
[48] J.R. Sohn, H.W. Kim, J. Mol. Catal. 52 (1989) 361.
[49] E.A. Paukshtis, N.S. Kotsarenko, V.P. Shmachkova, Catal. Lett. 69 (2000) 189.
[50] D. Spielbauer, G.A.H. Mekhemer, E. Bosch, H. Knözinger, Catal. Lett. 36 (1996) 59.
[51] M.A. Coelho, D.E. Resasco, E.C. Sikabwe, R.L. White, Catal. Lett. 32 (1995) 256.
[52] N. Lohitharn, J.G. Goodwin Jr., J. Catal. 245 (2007) 198.